Efficient recovery of phosphate from urine using magnesite modified corn straw biochar and its potential application as fertilizer

Yige Zhou, Zehui Liu, Jinhua Shan, Chengyang Wu, Eric Lichtfouse, Hongbo Liu

Journal of Environmental Chemical Engineering 12 (2024) 111925

https://doi.org/10.1016/j.jece.2024.111925

Efficient recovery of phosphate from urine using magnesite modified corn straw biochar and its potential application as fertilizer

Yige Zhou [a], Zehui Liu [a], Jinhua Shan [a], Chengyang Wu [a], Eric Lichtfouse [b,1], Hongbo Liu [a,*]

[a] School of Environment and Architecture, University of Shanghai for Science and Technology, 516 Jungong Road, 200093 Shanghai, China
[b] State Key Laboratory of Multiphase Flow in Power Engineering, Xi'an Jiaotong University, Xi'an, Shaanxi 710049 China

ARTICLE INFO

Editor: André Bezerra dos Santos

Keywords:
Modified biochar
Phosphate recovery
Human urine
Straw residue
Carbon emission reduction

ABSTRACT

Conventional phosphate fertilization is costly, carbon intensive, induces water pollution, and depletes natural phosphate ores, calling for alternative circular sources such as recycling phosphate from urine. However, actual phosphate adsorbents are moderately efficient and generate additional waste. Magnesite-modified biochar was synthesized by co-pyrolysis of corn straw and magnesite, which was used to adsorb phosphate in simulated urine. We compared the properties with other magnesium-based biochar materials and conducted pot experiments to assess feasibility of the saturated magnesite-modified biochar using as an alternative phosphate fertilizer. The results showed that the maximum adsorption capacity of magnesite-modified biochar for phosphate in urine was 176.16 mg/g, with the primary adsorption mechanisms involving electrostatic attraction and ligand exchange. Pot experiments showed that after 21 days, the germination rate and plant height of plants were 5.0–5.8 and 9.4–10.0 times respectively higher than those of plants in soil without biochar application. Overall, the prepared magnesite-modified biochar promises as an adsorbent with dual benefits in water treatment and phosphorus recovery. The saturated magnesite-modified biochar is proved as a good alternative phosphate fertilizer with carbon fixation, emission reduction and phosphorus cycling functions.

1. Introduction

The widespread utilization of conventional phosphate fertilization has resulted in the exhaustion of non-renewable phosphate rock reserves. Furthermore, the manufacturing process of conventional phosphate fertilizers generates substantial quantities of by-product phosphogypsum, which presents potential environmental hazards to both human health and the ecosystem [1]. The excessive application of phosphate fertilizers can lead to serious environmental problems [2]. Therefore, from the perspective of environmental protection and resource utilization, there is a need for more sustainable sources of phosphate fertilization [3]. In particular, urine contains relatively less organic matter and is rich in nitrogen, phosphorus and potassium [4]. Although urine produces only 1% of the total domestic wastewater in volume, It contributes more than 90% of the potassium, 80% of the nitrogen, and 50% of the phosphorus to the wastewater [5]. Raw urine is phytotoxic and thus cannot be used immediately as fertilizer for plant growth [6]. As a consequence, management of urine is costly and usually requires more than six months of storage before being applied to soils [7]. Moreover, variations in temperature, pH and time change the composition of urine, resulting in unstable urine composition [8,9], calling for alternative ways to recycle phosphorus.

The crop straw production in China has reached millions of tons per year [10,11]. Burning straw in the open air not only harms the environment and wastes resources, but also brings about greenhouse gas emission, calling for the recycling of waste straws [12]. Biochar converted from straws can be applied to soil to sequester carbon dioxide (CO_2) and improve soil conditions at the same time [13]. In this case it could mitigate CO_2 emissions from organic waste decomposition and increases carbon storage capacity of the soil [14].

Compared to other phosphorus-containing wastewater, the concentration of phosphate in urine is higher, in the range of 470–1070 mg/L [15]. The main methods to recover phosphorus from urine are ion exchange, adsorption, and chemical precipitation [16]. Adsorption is used extensively in wastewater phosphorus separation and recovery because of its ease of use, high performance, and low cost [17–19]. Biochar is an efficient adsorption material commonly used to adsorb pollutants and recover nutrients from water, due to its excellent cost-effectiveness, high

* Correspondence to: 516, Jungong Road, 200093 Shanghai, China.
E-mail address: Liuhb@usst.edu.cn (H. Liu).
[1] ORCID: 0000-0002-8535-8073

porosity, and strong ion adsorption performances [20,21]. Biomass such as straw and solid waste, wood, municipal sludge and manure are used as the main raw material for biochar preparation [22]. So far recovery of nutrient, humus, and metal ions by biochar has been the main research topics [23].

Although biochar is easy to prepare and has relatively good adsorption capacities, it is generally less efficient in its raw form conditions when recovering phosphate from water [24]. Indeed, the negatively-charged surface of biochar under neutral conditions is not favorable to adsorb negatively-charged phosphate ions, which highly limits the application of biochar in purification processes [25]. This issue can be solved by the functionalization of biochar surface to tune active sites and structural properties. In particular, the biochar surface can be modified by magnesium (Mg) materials. Indeed, Mg as an element is abundant in nature, and Mg^{2+} is considered as a suitable cation for phosphorus recovery [26,27]. Biochar modified with magnesium could fully absorb phosphate on its surface and the used biochar could be used as a valuable fertilizer. Therefore, in this study, we hypothesized that Mg-biochar could efficiently adsorb urine phosphate, and that urine-treated Mg-biochar could enhance plant growth.

A modified biochar called 'Mg-biochar' was prepared to recover phosphate from urine by mixed co-pyrolysis method in this study, using magnesite as the metal Mg source and waste corn straw as the carbon source. The adsorption mechanism and adsorption efficiency of Mg-biochar on phosphate in urine were investigated by characterization tools and adsorption experiments, and compared with other Mg-biochars. The urine-treated Mg-biochar was then used in potting experiments to verify its feasibility as an alternative phosphate fertilizer. Finally, the economic feasibility of Mg-biochar was evaluated.

2. Materials and methods

2.1. Materials and chemicals

The corn straw used to make biochar was provided by the Huifeng straw facility in Jiangsu Province, China. The straw was cut with scissors to roughly 100 meshes before being cleaned with deionized water repeatedly, put in a clean container, and then dried overnight at 60 ℃ in the oven. The magnesite used in the experiment was provided by the Honghu mining industry, Hubei Province, and is white or light yellow in color. The magnesite ore was rinsed three times by deionized water, grounded, 100 mesh sieved, and then dried at 60 ℃.

Total phosphorus (TP) content of the simulated urine was prepared with reference to the composition of human urine, with a concentration of roughly 140 mg/L. The human urine was obtained from a toilet of USST (University of Shanghai for Science and Technology). Due to the unstable nature of the fresh urine, simulated urine was used in subsequent adsorption sequential batch experiments. Based on monitoring results of the real urine, the simulated urine was prepared as shown in (Supplementary material Table S1).

2.2. Preparation of the Mg-biochar

10 g of 2/1 (mass: mass) magnesite powder and straw mixture were placed in a quartz boat and then pyrolyzed for 3 h at a temperature of 700 ℃ under dinitrogen protection in a tube furnace. After cooling, the modified biochar (Mg-biochar) was stored in a clean container. The pristine biochar (control) was prepared by the same procedure as the modified biochar.

2.3. Characterization of the study biochar

A scanning electron microscope (SEM) (Hitachi s4800, Japan) was used to observe changes in the morphology and structure of the study biochars. The X-ray diffraction (XRD) (Bruker D8 ADVANCE), Germany was applied to analyze the crystal structure of the study biochars. The change in binding energy of the primary components of modified biochar before and after adsorption was measured using X-ray photoelectron spectroscopy (XPS) from Thermo Scientific k-alpha, USA [28].

2.4. Adsorption experiments

To investigate the adsorption capacity of Mg-biochar on phosphate in urine under different initial pH conditions, 0.1 mol/L of hydrogen chloride or sodium hydroxide were added to condition the pH to 3.0–11.0. In addition, the point of zero charge (pH_{pzc}) of Mg-biochar was measured to explain the effect of initial pH on adsorption. The measurement steps can be found in (Supplementary Material Text S2).

kinetic experiments: dosage of the Mg-biochar was set at 1 g/L and the initial phosphorus concentration was set at 140 mg/L. Samples were taken at 0 min, 10 min, 20 min, 40 min, 60 min, 2 h, 4 h, 6 h, 8 h, 12 h, and 24 h of the reaction respectively.

Isotherm experiments: the simulated urine was diluted and the phosphorus content of the sample solution was adjusted in the range of 28.0–280.0 mg/L. A centrifuge tube containing 50 mL of suspension samples was shaken for 24 h at 25 °C and 125 rpm. A certain amount of the sample solution after reaction was passed through a 0.45 μm pore size filter membrane, and the quantity of total phosphorus in the filtrate was determined at 700 nm using a UV-Vis spectrophotometer.

According to Eqs. 1 and 2, the following was calculated to evaluate phosphate adsorption capacity and recovery rate of the study biochars [28]:

$$Q_e = V/M(C_i - C_e) \quad (1)$$

$$R_R(\%) = (C_i - C_e)/C_i \times 100 \quad (2)$$

Where Q_e stands for the quantity of phosphorus adsorbed per unit mass of biochar in mg/g, V for the solution's volume in L, M for the quantity of biochar dosed in g, C_i for the original phosphorus content in mg/L, C_e for the steady state phosphorus content in mg/L, and R_R for the recovering efficiency of phosphate in %w.

2.5. Kinetic and isothermal adsorption models

The kinetic model: pseudo-first-order and pseudo-second-order equations, intra-particle diffusion models were applied to study the kinetics of phosphorus adsorption from simulated urine by Mg-biochar and pristine biochar (control) at different contact times (0–24 h), and correlation coefficients were used to determine the applicability of each equation.

The isothermal adsorption model: examining the adsorption performance of Mg-biochar and pristine biochar (control) on phosphate at different initial phosphate concentrations. The experimental data of phosphorus adsorption by biochar were fitted using the Sips, Temkin, Freundlich, and Langmuir equations respectively.

The fitting of experimental data on phosphorus adsorption from urine by the Mg-biochar and pristine biochar (control) could refer to (Supplementary material Table S2).

2.6. Pot experiments

The soil used for pot experiments was the common clay from Handan, Hebei Province, China, with neutral pH and a density of 1.3 g/cm^3. Cabbage and ryegrass seeds were used for pot experiments. Square seedling (6 ×6 cm) pots with 8 cm in height were planted with 20 seeds of cabbage or ryegrass, and the soil dry weight was 374.4 g per pot. Experimental groups included 1) a control without biochar dosage, 2) the raw Mg-biochar dosage group, and 3) the urine-treated Mg-biochar dosage group. Each group of experiments was repeated three times, with a total of 18 potted plants. Mg-biochar materials were mixed with soils to obtain a concentration of 0.53 g biochar per Kg of soil. Each pot was

watered with 10 mL of drinking water daily, and the plant growth was measured after 21 days. The germination rate and plant height were measured, together with the content of nitrogen and phosphorus in the soil. Detailed descriptions of the measurement methods could refer to (Supplementary Material Text S3).

To assess the feasibility of urine-treated Mg-biochar as an alternative phosphorus fertilizer, potting experiments were conducted. Three sets of cultivated soil, including a control soil without biochar, a soil with raw Mg-biochar, and a soil with urine-treated Mg-biochar, were used to grow cabbage and ryegrass. After 21 days, P and N contents in soil were measured to evaluate plant nutrient uptake.

3. Results and discussion

3.1. Biochar properties

The morphology of pristine biochar, Mg-biochar and Mg-biochar after adsorption of simulated urine was analyzed by scanning electron microscopy (SEM, Fig. 1a-c). Results show that the pristine biochar has a well-developed pore structure originating from the evaporation of water and the decomposition of organic matter under high temperature pyrolysis conditions. The pristine biochar has a smooth surface made of a structural foundation based on carbon with few impurities. By contrast, the Mg-biochar surface shows granular impurities, which are MgO particles acting as key components for phosphate capture on surface of the modified biochar [29]. After suspension of the Mg-biochar in simulated urine for phosphate adsorption, the biochar surface becomes irregular with small pores and large lamellae on it, which could possibly result from the adsorption of phosphates on Mg-biochar cations.

X-Ray diffraction analysis of the raw Mg-biochar and urine-treated Mg-biochar reflects changes in the crystal structure of Mg-biochar (Fig. 2a). Results show typical MgO peaks at 37.1°, 43.1°, 62.4°, 74.8°, and 78.7°, which confirm the presence of magnesite in biochar. After urine treatment for the adsorption of phosphate, MgO peaks are still present and new peaks appear at 2θ of 16.0°, 20.6°, 29.3°, 32.0° and 36.9°, representing the hydrate of magnesium hydrogen phosphate according to [30]. New peaks also appeared at positions 27.2° and 33.3°, which is consistent with the crystal structure of struvite ($MgNH_4PO_4{\cdot}6\ H_2O$) [31]. These findings show that Mg-biochar adsorbed phosphate effectively.

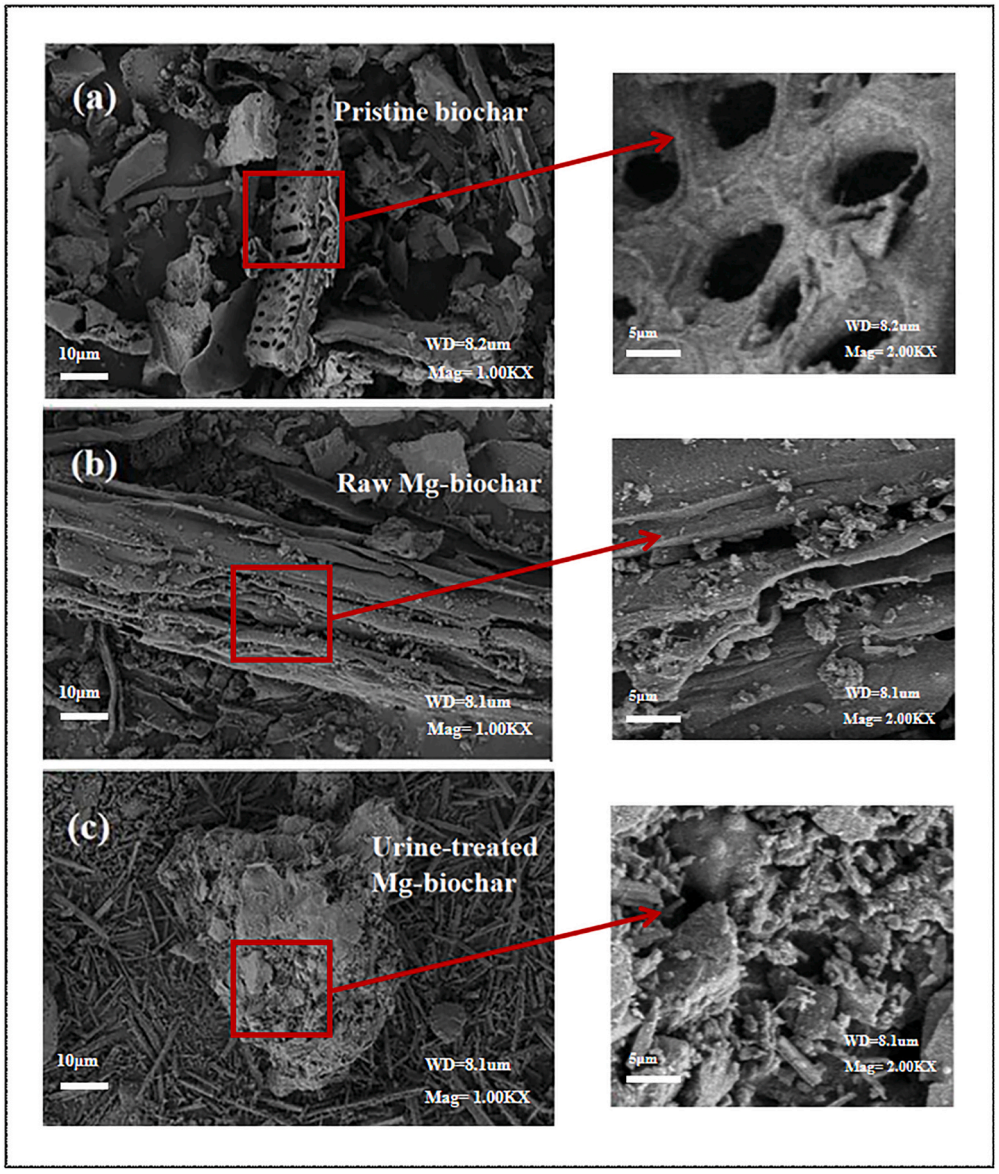

Fig. 1. Scanning electron microscopy (SEM) images of biochar by electron scanning microscopy at an operating voltage of 30 kV and a point resolution of 3.5 nm; pristine biochar (a), raw Mg-biochar (b), and urine-treated Mg-biochar (c).

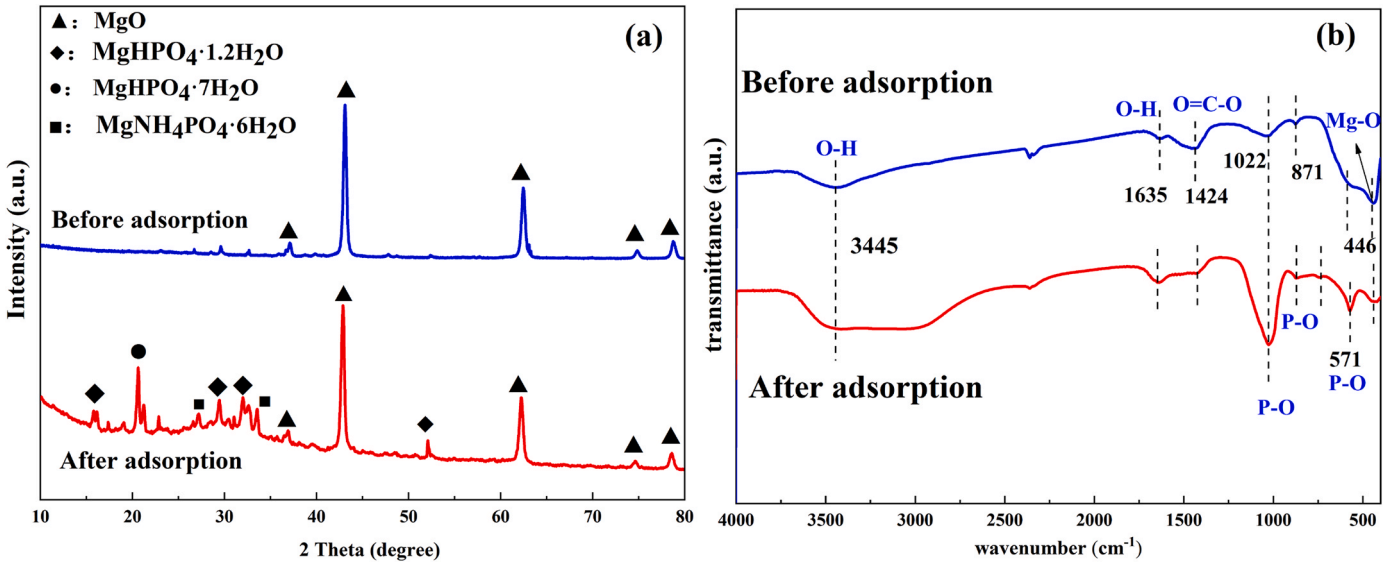

Fig. 2. (a): X-ray diffraction (XRD) of the raw Mg-biochar and the urine-treated Mg-biochar. The X-ray diffraction analysis was performed with CuKα as the source, with a voltage set to 40 KV, current to 40 mA, scan speed to 2°/min, scan angle to 10–80° and step size to 0.0359. (b): Fourier infrared spectra of raw Mg-biochar and urine-treated Mg-biochar at wavelengths from 500 to 4000 cm^{-1}.

Fig. 2b shows the Fourier infrared spectra of raw Mg-biochar and urine-treated Mg-biochar. Urine treatment induces wider peaks in O-H vibrational stretching at 3445 cm^{-1} and 1635 cm^{-1}, which could be interpreted by an increase of bound water and hydroxyl groups following the hydroxylation of MgO in water. Due to the vibration stretching of the P-O bond in HPO_4^{2-}/H_2PO_4, the peak values at 1022, 871, and 571 cm^{-1} significantly increased after urine treatment [32,33]. However, the peak of vibration stretching of Mg-O located at 446 cm^{-1}

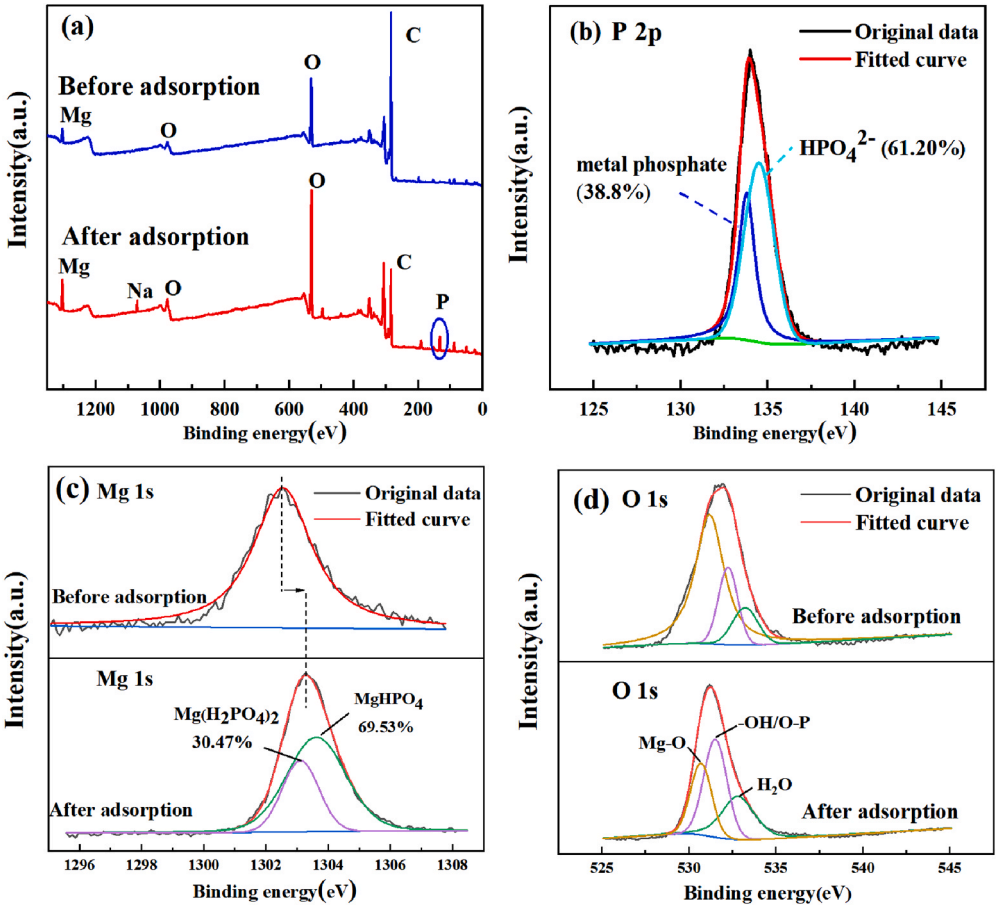

Fig. 3. Total X-ray photoelectron spectroscopy (XPS) spectra of raw Mg-biochar and urine-treated Mg-biochar (a) and P 2p fractionation spectrum (b), Mg 1 s (c), O 1 s (d). Measurement voltage is 12 kV with a filament current of 6 mA.

significantly decreased, once again proving that Mg-O is the main active site of Mg-biochar [34]. An infrared peak corresponding to O═C-O antisymmetric stretching vibration appeared at 1424 cm^{-1}, which may be attributed to the introduction of CO_3^{2-} during the Mg-biochar preparation process, as the main component of magnesite is $MgCO_3$. After urine treatment, it was found that the peak at 1424 cm^{-1} was significantly weakened, indicating that CO_3^{2-} was involved in the phosphate adsorption process [35]. Other studies also suggested that the exchange of CO_3^{2-} and phosphate anions via ion exchange is a pathway for phosphate removal. The obtained results indicate that the biochar adsorbed phosphorus successfully [36].

The results shown by X-ray photoelectron spectroscopy (XPS) indicated that the peaks of Mg, Na, C, O and P in urine-treated Mg-biochar were increased (Fig. 3a). The peak splitting of P 2p shows two peaks at 133.8 eV and 134.5 eV, corresponding to metal phosphate and HPO_4^{2-}, accounting for 38.8% and 61.2% respectively [37] (Fig. 3b). The literature indicates that there is a pathway for phosphate removal in metal modified materials: phosphate ions replace the hydroxyl groups of Mg-OH to form metal phosphates, indicating that ligand exchange is one of the main mechanisms for Mg-biochar to adsorb phosphate [38]. HPO_4^{2-} enters Mg-biochar through electrostatic attraction, intra-particle diffusion, or ion exchange, and then exhibits ionic form when detecting P 2p [39]. Peak splitting was also performed for Mg and O on biochar (Fig. 3c-d). Mg1s is shifted from 1302.6 eV to 1303.3 eV after adsorption. Splitting of Mg1s reveals two sub-peaks at 1303.1 eV and 1303.6 eV, responded to $Mg(H_2PO_4)_2$ and $MgHPO_4$, accounting for 30.5% and 69.5%, respectively. This further confirms the role of MgO in phosphate adsorption in Mg-biochar, and once again confirms that ligand exchange is one of the important adsorption mechanisms. The O1s peak can be divided into three sub-peaks with a binding energy of 530.7 eV corresponding to Mg-O, a binding energy of 531.5 eV for -OH/P-O and 532.8 eV for H_2O [40]. Following phosphate adsorption, the percentage of the peak area representing Mg-O decreases from 67.9% to 28.1%, which is primarily caused by phosphate ions binding to Mg and occupying the original Mg-O site [41]. In addition, the percentage of peak area representing -OH/P-O increased from 19.7% to 42.1%, mainly due to the adsorption of phosphate ions in the aqueous solution by biochar. The peak of H_2O increased from 12.4% to 29.8%, mainly because biochar increases the bound water on its surface through the adsorption process.

Overall, our findings confirm the successful synthesis of Mg-biochar and adsorption of phosphates from simulated urine by Mg-biochar.

3.2. *Effect of initial pH and contact time*

The effects of Mg-biochar on phosphate adsorption and recovery in urine under different initial pH conditions was investigated (Fig. 4a, c). We found that the adsorption capacity of magnesium biochar for phosphate reached a maximum of 118.8 mg/g from 73.2 mg/g within the initial pH range of 3.0–7.0, and the recovery rate increased from 52.3% to the maximum of 88.0%. The adsorption capacity and recovery rate remained basically stable within initial pH range of 7.0–9.0 [42]. These phenomena indicate that increasing the pH of the solution within a certain range is beneficial for the removal of phosphate. However, the absorption capacity and recovery rate significantly decreased within initial pH range of 9.0–11.0. At pH= 11.0, the adsorption capacity of phosphate decreased to 68.1 mg/g, and the recovery rate decreased to 48.7%. The pH affects the adsorption capacity and recovery by controlling the phosphate morphology and the surface properties of Mg-biochar [43]. In pH range of 3.0–7.2, phosphate in urine mainly exists in the form of $H_2PO_4^-$, while HPO_4^{2-} is the main form in the pH range of 7.0–9.0 [44]. Compared with $H_2PO_4^-$, Mg-biochar is easier to capture HPO_4^{2-} [45]. Therefore, as the initial pH increases within the range of 3.0–7.0, $H_2PO_4^-$, is converted into HPO_4^{2-}, and the phosphate adsorption capacity and recovery rate of Mg-biochar increase. Point of zero charge (pH_{pzc}) of Mg-biochar was detected to be 9.9. When the pH

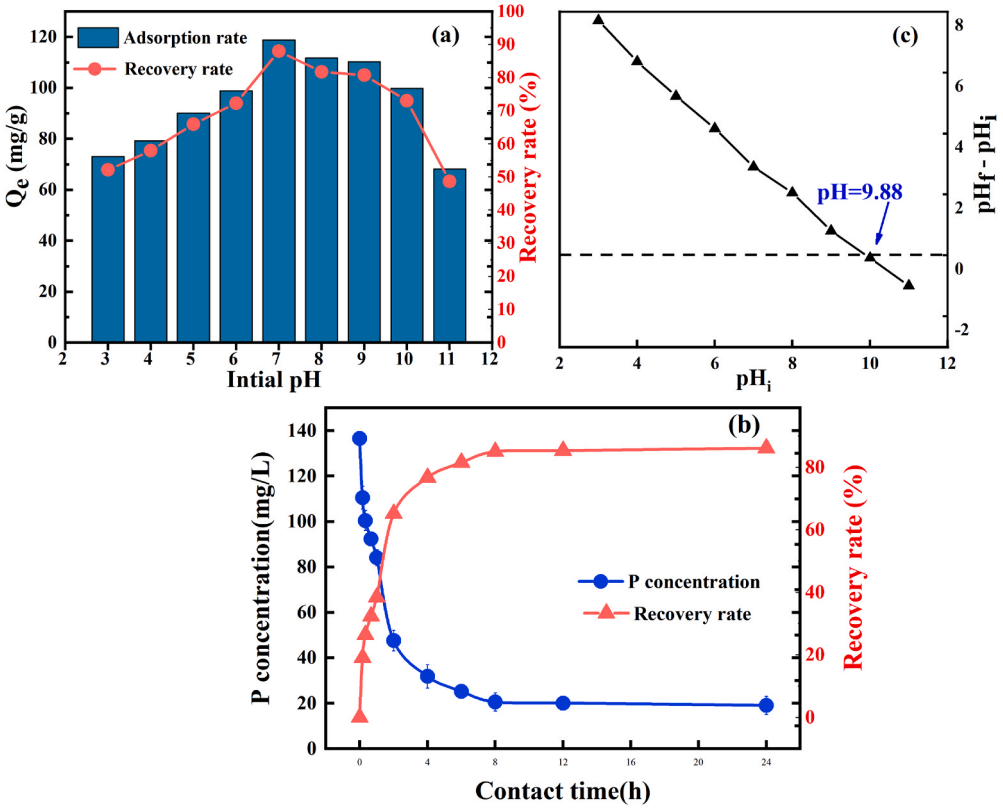

Fig. 4. Adsorption capacity and recovery of phosphate in urine by the Mg-biochar under different initial pH conditions (a), and phosphate recovery from urine by Mg-biochar under different contact times (b).

value of the solution surpasses 9.9, the Mg-biochar surface carries negative charge, which causes electrostatic repulsion with phosphate ions. Additionally, OH^- in the solution competes with phosphate ions for adsorption, further decreasing the adsorption capacity and removal rate of phosphate ions. Therefore, the adsorption capacity and removal rate of phosphate decrease as the initial pH increases in the range of 9.0–11.0 [38].

The effect of contact time on the recovery of phosphate in urine by Mg-biochar is shown in Fig. 4b. The adsorption rate of phosphate in urine recovered by Mg-biochar was fast. In the first 1 h, a large number of adsorption sites existed on the surface of Mg-biochar which rapidly captured phosphate ions by electrostatic attraction, and the P concentration was reduced to 84.0 mg/L, with a recovery rate of 38.5% [46]. Subsequently, the decrease of P concentration slowed down. This was because the adsorption sites were gradually occupied and the adsorption of phosphate was weakened. After 8 h of reaction, the adsorption of phosphate by biochar reached the adsorption equilibrium state with a recovery efficiency of 85.3% [47].

3.3. *Phosphate recovery performance and mechanism of the Mg-biochar*

By kinetic fitting, we studied the mechanism of adsorption of phosphate in urine on Mg-biochar (Fig. 5a-b, Table S3). Adsorption kinetics is one of the key factors evaluating the efficiency of adsorbents. It can be observed that both pseudo-first-order and pseudo-second-order kinetic model can well describe the kinetic behavior of Mg-biochar adsorption of phosphate in urine, with R^2 values reaching above 0.97. The maximum adsorption capacity of pseudo-second-order kinetic model can reach 127.8 mg/g, which is closer to the true adsorption value, and R^2 is also higher, reaching 0.988. This indicates that the adsorption process is mainly chemical adsorption, which is consistent with the analysis of others [39,47]. Combining the results of XPS, XRD, and effect of initial pH, it is once again confirmed that MgO on biochar plays a crucial role in the adsorption process. The electrostatic attraction process and ligand exchange process are the main mechanisms for Mg-biochar to adsorb phosphate [48]. The R^2 value of pseudo-first-order kinetic model is relatively high, indicating that Mg-biochar can also have a certain physical adsorption effect on phosphate [49]. The adsorption capacity of Mg-biochar significantly increased within 0.5 h, and gradually reached equilibrium after 5 h [50]. Compared with Mg-biochar, the maximum adsorption capacity of pristine biochar (control) is 1.29 mg/g, which can be ignored (Fig. 5c, Table S4). The reason may be that the surface of pristine biochar (control) is usually negatively charged, and there is a repulsive effect with negatively charged phosphates, resulting in weak adsorption [48,51]. Analyzing the kinetic curves of the pristine biochar, both pseudo-first-order and pseudo-second-order kinetic model cannot achieve good expression. Within 0.5 h, there was a slight increase in adsorption capacity, which combined with the pseudo-first-order kinetic model (R^2 =0.84), is speculated to be due to the physical adsorption effect of the pristine biochar [42]. However, after 5 h, the adsorption capacity showed a decreasing trend, suggesting the presence of trace dissolution of P from pristine biochar [29,43].

The intra-particle diffusion model analysis of Mg-biochar adsorption phosphate data conforms to the three-stage separation method [52]. The first stage has a high k_{p1} value (k_{p1}=51.94), indicating rapid diffusion of phosphate on the surface of Mg-biochar [37]. The second stage belongs to mesoporous diffusion, and the adsorption rate is mainly controlled by intra particle diffusion. The k_{p2} value (k_{p2}=19.47) is significantly lower than k_{p1}, indicating that most of the surface-active sites of Mg-biochar are occupied, and phosphate gradually diffuses into the interior of Mg-biochar [28]. The third stage belongs to microporous diffusion, and $k_{p3} < 1$ indicates that adsorption equilibrium has gradually been reached. Observing the three stages, it can be found that none of them have passed through the origin (C‡0), indicating that the adsorption of phosphate in urine by Mg-biochar involves intra-particle diffusion process, but is controlled by multiple processes [53]. In addition, the high C value indicates that the boundary layer of Mg-biochar will greatly affect the adsorption of phosphate[37].

We also investigated the mechanism of phosphate adsorption on Mg-biochar by isothermal fitting using Langmuir, Freundlich, Sips, and Temkin models in the urine matrix (Fig. 6a, Table S3). The correlation coefficient of Sips for Mg-biochar is 0.97, Langmuir is 0.95, Temkin is 0.92, and Freundlich is 0.82. Indeed, the Langmuir model is often used to describe monolayer adsorption processes, whereas Freundlich and Temkin models describe mainly bi-layered and multilayered adsorption processes [54]. And the Sips model is an improvement of the Langmuir model and the Freundlich model [55]. Sips, Langmuir, and Temkin models fitted the adsorption data well (R^2 >0.9), while the Freundlich model had the worst fit, indicating that the model was not suitable for the adsorption process. The highest fitting of the Sips model indicates that adsorption is carried out through physical and chemical adsorption,

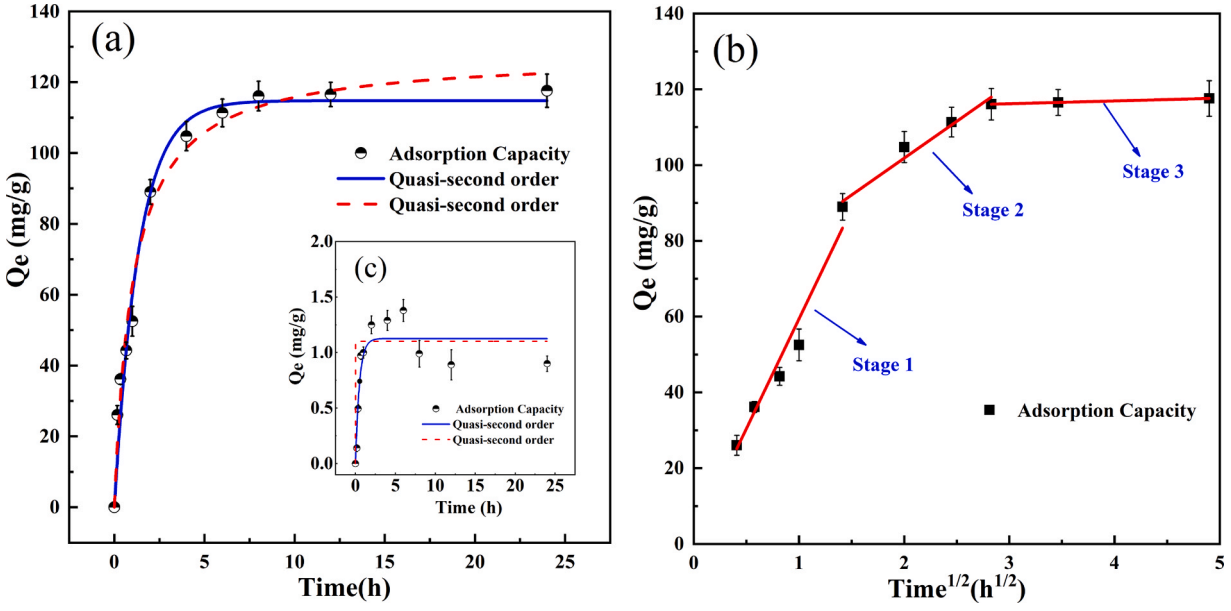

Fig. 5. Pseudo-first-order, pseudo-second-order kinetic curves of Mg-biochar (a), Intra-particle diffusion model of Mg-biochar (b) and pristine biochar (control) (c).

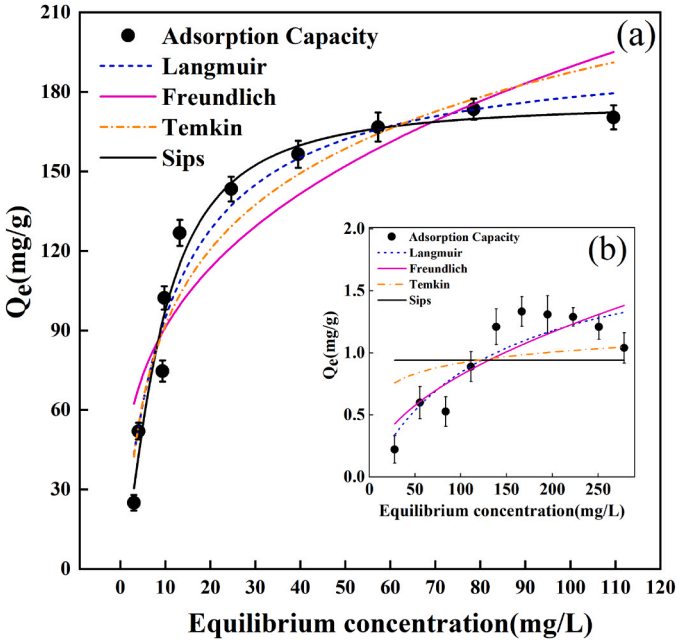

Fig. 6. Adsorption isotherms of phosphate adsorption by Mg-biochar (a) and pristine biochar (control) (b).

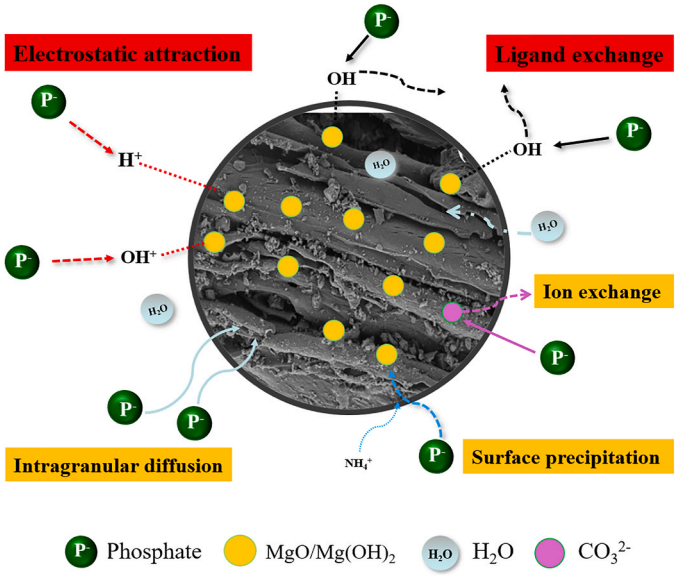

Fig. 7. Recovery mechanism for phosphate by Mg-biochar.

with phosphate in close contact with the surface of Mg-biochar MgO, which is consistent with the kinetic fitting results. The theoretical maximum phosphate adsorption capacity of 176.16 mg/g obtained by using Sips model for Mg-biochar is much higher than the average adsorption capacity of 28.90 mg/g reported by other researchers for virgin biochar, and also outperformed the average adsorption capacity of 143.10 mg/g for the modified biochar [56]. However, the pristine biochar (control) cannot be well expressed by other isothermal adsorption models except for Langmuir and Freundlich (Fig. 6b, Table S4). However, the maximum theoretical adsorption capacity of Langmuir is only 1.34 mg/l (R^2 =0.71), which can be ignored compared to the adsorption capacity of Mg-biochar. The Freundlich model can express the adsorption of phosphate in urine by pristine biochar (R^2 =0.95), indicating that its adsorption of phosphate in urine usually occurs on a non-uniform surface [57]. Studies have shown that the higher the K_F value, the stronger the material's ability to adsorb pollutants [58]. The K_F value of pristine biochar is only 0.15, indicating its weak ability to adsorb phosphate. Overall, as a control group, the adsorption of phosphate in urine by pristine biochar belongs to physical adsorption, which conforms to the pseudo first-order kinetic model and occurs on non-uniform surfaces.

The proposed recovery mechanism of Mg-biochar for phosphate is shown in (Fig. 7), including the following mechanisms. (1) Electrostatic attraction. It is a hydration reaction between Mg-biochar and aqueous solution, which generates a large number of protonated hydroxyl groups (OH_2^+, OH^+) at an appropriate solution pH to attract negatively charged phosphate ions. (2) Ligand exchange. The Mg-biochar hydrates on the surface of urine aqueous solution to generate Mg-OH, and phosphate ions replace the hydroxyl groups of Mg-OH to form metal phosphates. The adsorption capacity of biochar for phosphate is thus enhanced through ligand exchange. (3) Surface precipitation. The prepared artificial urine contains phosphate ions and trace amounts of NH_4^+; under certain conditions, struvite crystallization will form on the surface of Mg-biochar.

The analysis of intra-particle diffusion model shows that the adsorption of phosphate in urine by Mg-biochar can be divided into three stages. Firstly, phosphate ions are quickly captured by the adsorption sites on the surface of the adsorbent. Then, after the adsorption site is saturated, it diffuses into the interior of Mg-biochar through intra-particle diffusion, and finally reaches adsorption equilibrium through internal microporous diffusion. The CO_3^{2-} introduced during the formation of Mg-biochar exchanges with phosphate ions in urine, thereby improving the phosphate recovery rate. The introduction of CO_3^{2-} is related to the modifier magnesite, whose main form is $MgCO_3$.

In terms of raw material acquisition, the preparation of Mg-biochar is mostly based on wastes, which enables the resource utilization of wastes (Table 1). It is more difficult to obtain the garden waste mixture of Populus X Canadensis Moench and Sophora japonica Linn than obtaining straw waste [59]. China produces millions of tons of straw annually, and the preparation of biochar from straw and its eventual return to the field as an alternative fertilizer is an effective strategy for carbon sequestration, emission reduction and waste resource utilization, which is in line with the theme of green development. Analyzing the preparation method, Shin et al. used a one-step method to prepare Mg-biochar. The biomass was soaked in $MgCl_2$ solution for 8 h, and then dried and pyrolyzed to obtain Mg-biochar [29]. Of course, there is another method to prepare Mg-biochar in two steps. First, biochar was obtained by pyrolysis. Then the biochar is modified by soaking modifier and further pyrolyzed [39]. Both methods are undoubtedly long and tedious. In contrast, in this study, Mg-biochar was prepared more simply by directly mixing and co-pyrolyzing magnesite and straw powder without the need for a long soaking or drying step. Based on the maximum adsorption capacity analysis, the adsorption capacity of Mg-biochar for phosphate varied greatly. This may be related to the modification conditions of the biochar, such as pyrolysis temperature and type of modifier [60]. The maximum adsorption capacity of Mg-biochar obtained by Liang et al. by soaking peanut shell powder in Mg $(NO_3)_2$ solution was 1809 mg/g, which is undoubtedly huge [61]. However, the modifier Mg $(NO_3)_2$ is an explosive and hazardous chemical, making it a very dangerous preparation method. On the contrary, we used magnesite, which is very stable in nature. In addition, magnesite tailings are a cheap magnesite resource, which can also further reduce the cost of the modification and improve the economic feasibility and competitiveness of Mg-biochar.

Compared with other studies, Mg-biochar prepared in this study has the advantages of easy availability of raw materials, simple preparation method, and economic safety. It also has good phosphate adsorption properties, which can realize the dual benefits of water treatment and phosphorus recovery [62]. In addition, the use of urine-treated Mg-biochar as an alternative phosphorus fertilizer not only achieves carbon sequestration and emission reduction, but also further promotes

Table 1
Comparison of phosphate adsorption by Mg-biochar in this and other studies.

Raw material	Temperature (°C)	Modifier	Q_e (mg/g)	Process	References
Bagasse	800	Sepiolite	128.12	One-step method	[52] Deng et al.
Aspen and locust wood	600	$MgCl_2$	119.95	One-step method	[43] Xu et al.
Corn straw	700	Magnesite solid	176.16	Co-pyrolysis	This study
Peanut shell	800	Mg $(NO_3)_2$	1809	One-step method	[61] Liang et al.
Leaf, saw dust, and straw	600	$C_4H_{14}MgO_8$	121.95	One-step method	[64] Luo et al.
Tomato leaves	600	Hoagland solution of magnesium	13.3	One-step method	[65] Yao et al.
Corncob	800	$MgCl_2$	8.55	One-step method	[66] Jena et al.
Coffee grounds	500	$MgCl_2$	63.5	One-step method	[29] Shin et al.
Mixed wood waste	600	$MgCl_2$	116.4	One-step method	[48] Xu et al.
Corn	600	$MgCl_2$	239	One-step method	[42] Fang et al.
Mixed wood waste	600	$MgCl_2$	118	One-step method	[59] Liu et al.
Tea leaves	650	$MgCl_2$	58.80	Two-step method	[39] Feng et al.

phosphorus recycling [63].

3.4. Feasibility study of urine-treated Mg-biochar as an alternative phosphate fertilizer

3.4.1. Changes in soil properties

Fig. 8a-b indicate that P contents in the soil increased after applying raw Mg-biochar for 21 days. P contents in the soils of cabbage and ryegrass rose from 0.87 mg/g and 1.28 mg/g comparing to the control of 1.15 mg/g and 1.28 mg/g, respectively. Previous studies have revealed that soil microbes amplify the phosphorus-releasing effect [67]. Another explanation is that plant roots and root exudates contain phosphorus compounds, and biochar promotes an increase in P concentration by promoting plant growth [32]. After 21 days of applying urine-treated Mg-biochar, P concentration in the soil notably increased from 0.78 mg/g in the control group to 2.19 mg/g in the cabbage group and 2.62 mg/g in the ryegrass group. This increase is equivalent to 2.81 to 3.36 times the P content in the control group. These results suggest that urine-treated Mg-biochar releases large amounts of adsorbed phosphate into the soil, ultimately resulting in a significant rise in P concentration. Both the application of raw Mg-biochar and urine-treated Mg-biochar showed a slight increase in soil NH_4^+ content. Compared with using raw Mg-biochar, urine-treated Mg-biochar exhibited higher NH_4^+ concentration. The formation of a small quantity of struvite crystallization on the surface of Mg-biochar during the phosphate adsorption process might be the cause. Incorporating urine-treated Mg-biochar to the soil after a period of time, the struvite crystallization on the surface of biochar will slowly dissolve and release N elements [68]. This is consistent with the results of XRD, further indicating that Mg-biochar may produce a minor quantity of struvite crystallization when adsorbing phosphate in urine.

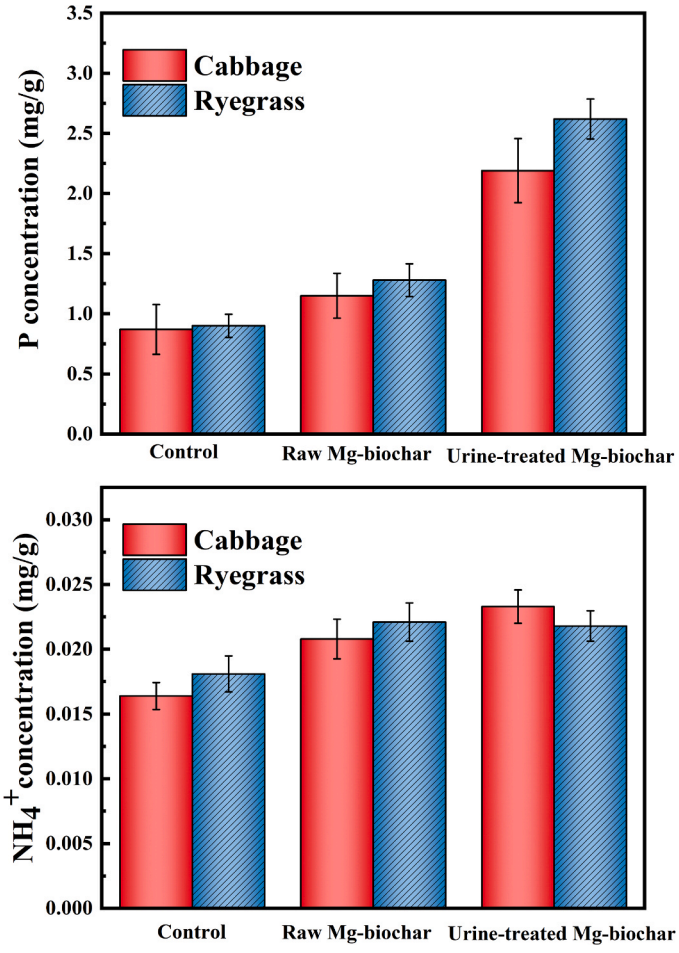

Fig. 8. P contents (a) and NH_4^+ contents (b) in cultivated soils without biochar (control), with raw Mg-biochar and with urine-treated Mg-biochar.

3.4.2. Changes in plant growth

After a 21-day cultivation, we measured the germination rate and average plant height of cabbage and ryegrass to evaluate the impact of urine-treated Mg-biochar on plant growth, as presented in (Fig. 9, Table 2). Germination rate of control cabbage and ryegrass without biochar were approximately 13.3%, which we hypothesize could be attributed to unfavorable temperature and planting conditions. Laboratory temperatures ranged from 7–15 °C during winter planting experiments, which led to decreased plant germination rates [69,70]. Furthermore, the soil used for planting was a typical clay soil from Hubei Province with high organic matter content but poor permeability,

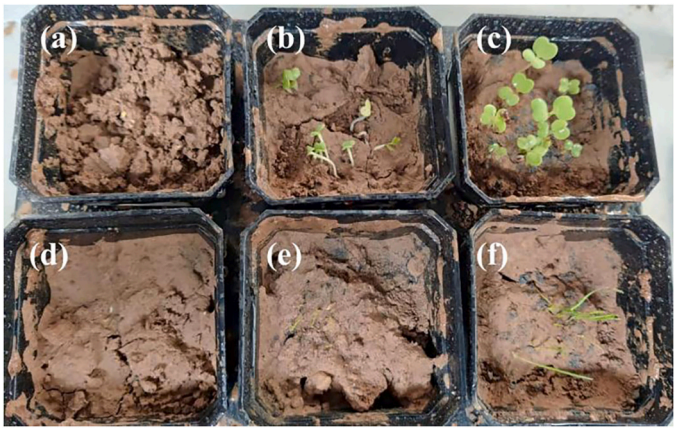

Fig. 9. Growth of cabbage in cultivated soils without biochar (a), with raw Mg-biochar (b) and with urine-treated Mg-biochar (c). Growth of ryegrass in cultivated soils without biochar (d), with raw Mg-biochar (e) and with urine-treated Mg-biochar (f).

Table 2
Plant growth under different biochar application conditions.

The experimental group	Control	Raw Mg-biochar	Urine-treated Mg-biochar
Germination rate (%)			
Cabbage	13.3 ± 2.9	43.3 ± 2.9	66.7 ± 1.1
Ryegrass	13.3 ± 5.8	48.3 ± 7.6	76.7 ± 1.5
Plant height (cm)			
Cabbage	0.19 ± 0.04	1.4 ± 0.2	1.9 ± 0.3
Ryegrass	0.31 ± 0.02	1.1 ± 0.2	2.9 ± 0.4

resulting in challenges for the crops to take root [71]. Therefore, careful consideration of soil selection is essential in promoting plant germination rates. In the experimental group treated with raw Mg-biochar, the germination rates of cabbage and ryegrass were 43.3% and 48.3%, respectively. These rates were significantly higher, by 3.26 and 3.63 times respectively, as compared to the control group. This observed increase in germination rates can be attributed to the ability of biochar to prevent soil nutrient loss and enhance water absorption, thus promoting plant growth and development [72]. The germination rates of cabbage and ryegrass in the group treated with urine-treated Mg-biochar increased significantly to 66.7% and 76.7%, respectively, which were 5.02 and 5.77 times higher than those in the control group. This improvement was mainly attributed to the addition of external phosphorus, particularly the use of urine-treated Mg-biochar, which enhances plant growth and development. This finding demonstrates that Mg-biochar effectively absorbs phosphate from urine with high bioavailability [73]. The mean plant height and germination results were comparable. Significantly greater plant growth was observed with the introduction of raw Mg-biochar when compared to the control. Nevertheless, with urine-treated Mg-biochar, the increase in plant height was substantially greater, reaching 9.4–10.0 times that observed in the control group. These findings indicate that urine-treated Mg-biochar presents a practical and effective alternative to phosphate fertilizer [74].

3.5. *Economic feasibility of Mg-biochar*

Burning straw in the fields can produce particulate matter that harms people's lungs [75]. Studies have shown that converting straw waste to biochar can reduce the amount of CO_2 emitted into the atmosphere and reduce air pollution caused by field burning [76]. In addition, the use of biochar in agriculture can be effective in reducing the amount of greenhouse gases emitted to the atmosphere from soil tillage systems. Therefore, making biochar from straw waste is a good treatment strategy to minimize the environmental and health risks associated with straw waste disposal [77].

In order to fully assess the potential of using Mg-biochar as a phosphate adsorbent on a large scale, its environmental and economic benefits must be evaluated. Life Cycle Cost Analysis (LCCA) is a research tool that has been applied to analyze processes from a cost perspective in a variety of situations [78]. It allows one to understand whether the decisions taken will ensure sustainable economic development and thus to calculate more precisely the economic benefits of the process under consideration [79]. In this study, the cost of preparing Mg-biochar was analyzed using LCCA. The detailed calculations could refer to (Table S5, Text S3).

The production cost of Mg-biochar in this study was 2.6 USD/kg (excluding labor and packaging costs, etc.). This cost is significantly lower than the commercial biochar price of 11 USD/kg [80]. However, the cost of pyrolyzed pristine biochar would be lower. As observed in this paper, pristine biochar is typically unable to adsorb phosphate. In contrast, Mg-biochar proved to be a more cost-effective option due to its superior adsorption capacity [81]. And the main cost input lies in the use of magnesite. Therefore, in order to further improve the economic feasibility of Mg-biochar, the use of waste magnesite will be considered in the future to minimize the cost of modification. Another important component of biochar preparation cost is energy consumption. Factors such as holding time and pyrolysis temperature will be further adjusted in the future to further reduce the preparation cost. In addition, the use of biochar as an adsorbent in agriculture reflects the economic viability of biochar in a recycling system. For example, microalgae biochar prepared by Santos can also be used as a soil conditioner after adsorbing nutrients such as nitrogen and phosphorus from wastewater, thus reducing the need for fertilizers [82]. Tools such as LCA will be used in future studies to assess how much chemical fertilizer can be replaced, how much crop yields can be increased, and how much carbon emissions can be reduced by using Mg-biochar adsorbed with saturated phosphate as a phosphate fertilizer in agriculture in the study [83].

Overall, the cost of preparing Mg-biochar in this study was lower than the selling price of commercial biochar and more cost-effective due to its higher adsorption capacity. In the future, other waste materials that can be used as alternatives to magnesite modifiers, such as magnesium-containing tailings from bulk mining, will continue to be investigated in order to make Mg-biochar more economically viable for phosphate recovery. Beyond that, the focus of research will begin to shift to the practical application of Mg-biochar in the future.

4. Conclusion

Mg-biochar was successfully prepared by co-pyrolysis using corn straw as raw material and magnesite as modifier for the recovery of phosphate in urine. The results showed that MgO particles were the main active sites in the adsorption process of Mg-biochar. The adsorption mechanism of phosphate on Mg-biochar is an adsorption process dominated by chemical adsorption and supplemented by physical adsorption. The process mainly involves ligand exchange, electrostatic attraction, presence of intraparticle diffusion, ion exchange and surface precipitation. Compared with Mg-biochar in other studies, the Mg-biochar prepared in this study has the advantages of easy availability of raw material, simple preparation method, economical and safe production, and good phosphate adsorption performance (176.16 mg/g). Water treatment and phosphorus recovery can be performed simultaneously using Mg-biochar in this study. Saturated Mg-biochar can be used as a substitute for phosphate fertilizer to improve soil quality, increase soil phosphorus content, and promote the growth of cabbage and ryegrass. It also contributes to the sustainable use of waste resources, bringing about environmental and economic benefits. We have also assessed the economic feasibility of Mg-biochar. In the future, we will investigate the long-term effects on plants using urine-treated Mg-biochar as an alternative phosphorus fertilizer. In addition, we will evaluate and discuss the economics and low-carbon nature of Mg-biochar throughout its preparation, use, and reuse as a fertilizer using LCA and other methods. In conclusion, our study demonstrates a material that can recover phosphorus in wastewater and effectively increase phosphorus in soil.

CRediT authorship contribution statement

Yige Zhou: Lab investigations, mechanism study. **Zehui Liu:** Methodology, data curation. **Jinhua Shan:** Methodology, data curation. **Chengyang Wu:** Review & editing. **Eric Lichtfouse:** Review & editing. **Hongbo Liu:** Funding acquisition, conceptualization, project administration, supervision, draft manuscript.

Declaration of Competing Interest

The authors declare that they have no known competing financial interests or personal relationships that could have appeared to influence the work reported in this paper.

Data availability

Data will be made available on request.

Acknowledgments

This work was supported by the National Natural Science Foundation of China (No.52070130) and the Natural Science Foundation of Shanghai (No.22ZR1443200).

Appendix A. Supporting information

Supplementary data associated with this article can be found in the online version at doi:10.1016/j.jece.2024.111925.

References

[1] Z. Wang, X. Ma, H. Pan, X. Yang, X. Zhang, Y. Lyu, et al., Investigating effects of phosphogypsum disposal practices on the environmental performance of phosphate fertilizer production using emergy analysis and carbon emission amounting: a case study from China, J. Clean. Prod. 409 (2023), https://doi.org/10.1016/j.jclepro.2023.137248.

[2] C. Wang, D. Luo, X. Zhang, R. Huang, Y. Cao, G. Liu, et al., Biochar-based slow-release of fertilizers for sustainable agriculture: a mini review, Environ. Sci. Ecotechnology 10 (2022), https://doi.org/10.1016/j.ese.2022.100167.

[3] B. Sniatala, T.A. Kurniawan, D. Sobotka, J. Makinia, M.H.D. Othman, Macro-nutrients recovery from liquid waste as a sustainable resource for production of recovered mineral fertilizer: uncovering alternative options to sustain global food security cost-effectively, Sci. Total Environ. 856 (2023) 159283, https://doi.org/10.1016/j.scitotenv.2022.159283.

[4] C. Courtney, D.G. Randall, Concentrating stabilized human urine using eutectic freeze crystallization for liquid fertilizer production, Water Res. 233 (2023) 119760, https://doi.org/10.1016/j.watres.2023.119760.

[5] S.K.L. Ishii, T.H. Boyer, Life cycle comparison of centralized wastewater treatment and urine source separation with struvite precipitation: focus on urine nutrient management, Water Res. 79 (2015) 88–103, https://doi.org/10.1016/j.watres.2015.04.010.

[6] A. Pathy, J. Ray, B. Paramasivan, Challenges and opportunities of nutrient recovery from human urine using biochar for fertilizer applications, J. Clean. Prod. 304 (2021), https://doi.org/10.1016/j.jclepro.2021.127019.

[7] K.M. Udert, M. Wächter, Complete nutrient recovery from source-separated urine by nitrification and distillation, Water Res. 46 (2012) 453–464, https://doi.org/10.1016/j.watres.2011.11.020.

[8] A. Patel, A.A. Mungray, A.K. Mungray, Technologies for the recovery of nutrients, water and energy from human urine: a review, Chemosphere 259 (2020) 127372, https://doi.org/10.1016/j.chemosphere.2020.127372.

[9] D.G. Randall, M. Krähenbühl, I. Köpping, T.A. Larsen, K.M. Udert, A novel approach for stabilizing fresh urine by calcium hydroxide addition, Water Res. 95 (2016) 361–369, https://doi.org/10.1016/j.watres.2016.03.007.

[10] J. Xu, Z. Liu, J. Dai, Environmental and economic trade-off-based approaches towards urban household waste and crop straw disposal for biogas power generation project -a case study from China, J. Clean. Prod. 319 (2021), https://doi.org/10.1016/j.jclepro.2021.128620.

[11] W. Liu, C. Wang, A.P.J. Mol, Rural residential CO_2 emissions in China: where is the major mitigation potential? Energy Policy 51 (2012) 223–232, https://doi.org/10.1016/j.enpol.2012.05.045.

[12] X. Wang, L. Yang, Y. Steinberger, Z. Liu, S. Liao, G. Xie, Field crop residue estimate and availability for biofuel production in China, Renew. Sustain. Energy Rev. 27 (2013) 864–875, https://doi.org/10.1016/j.rser.2013.07.005.

[13] K. Januszewicz, P. Kazimierski, M. Klein, D. Kardaś, J. Łuczak, Activated carbon produced by pyrolysis of waste wood and straw for potential wastewater adsorption, Materials 13 (2020), https://doi.org/10.3390/ma13092047.

[14] D. Feng, S. Wang, Y. Zhang, Y. Zhao, S. Sun, G. Chang, et al., Review of carbon fixation evaluation and emission reduction effectiveness for biochar in China, Energy Fuels 34 (2020) 10583–10606, https://doi.org/10.1021/acs.energyfuels.0c02396.

[15] H. Bacelo, A.M.A. Pintor, S.C.R. Santos, R.A.R. Boaventura, C.M.S. Botelho, Performance and prospects of different adsorbents for phosphorus uptake and recovery from water, Chem. Eng. J. 381 (2020) 122566, https://doi.org/10.1016/j.cej.2019.122566.

[16] H. Huang, J. Li, B. Li, D. Zhang, N. Zhao, S. Tang, Comparison of different K-struvite crystallization processes for simultaneous potassium and phosphate recovery from source-separated urine, Sci. Total Environ. 651 (2019) 787–795, https://doi.org/10.1016/j.scitotenv.2018.09.232.

[17] M. Ahmad, A.U. Rajapaksha, J.E. Lim, M. Zhang, N. Bolan, D. Mohan, et al., Biochar as a sorbent for contaminant management in soil and water: a review, Chemosphere 99 (2014) 19–33, https://doi.org/10.1016/j.chemosphere.2013.10.071.

[18] G. Fang, C. Zhu, D.D. Dionysiou, J. Gao, D. Zhou, Mechanism of hydroxyl radical generation from biochar suspensions: implications to diethyl phthalate degradation, Bioresour. Technol. 176 (2015) 210–217, https://doi.org/10.1016/j.biortech.2014.11.032.

[19] L. Guo, A. Chen, N. He, D. Yang, M. Liu, Exogenous silicon alleviates cadmium toxicity in rice seedlings in relation to Cd distribution and ultrastructure changes, J. Soils Sediment. 18 (2018) 1691–1700, https://doi.org/10.1007/s11368-017-1902-2.

[20] W. Xiang, X. Zhang, J. Chen, W. Zou, F. He, X. Hu, et al., Biochar technology in wastewater treatment: a critical review, Chemosphere 252 (2020) 126539, https://doi.org/10.1016/j.chemosphere.2020.126539.

[21] S. Das, S.R. Paul, A. Debnath, Fabrication of biochar from jarul (Lagerstroemia speciosa) seed hull for ultrasound aided sequestration of ofloxacin from water: phytotoxic assessments and cost analysis, J. Mol. Liq. 387 (2023) 122610, https://doi.org/10.1016/j.molliq.2023.122610.

[22] X. Li, C. Wang, J. Zhang, J. Liu, B. Liu, G. Chen, Preparation and application of magnetic biochar in water treatment: a critical review, Sci. Total Environ. 711 (2020) 134847, https://doi.org/10.1016/j.scitotenv.2019.134847.

[23] H. Yang, S. Ye, Z. Zeng, G. Zeng, X. Tan, R. Xiao, et al., Utilization of biochar for resource recovery from water: a review, Chem. Eng. J. 397 (2020) 125502, https://doi.org/10.1016/j.cej.2020.125502.

[24] K. Vikrant, K.-H. Kim, Y.S. Ok, D.C.W. Tsang, Y.F. Tsang, B.S. Giri, et al., Engineered/designer biochar for the removal of phosphate in water and wastewater, Sci. Total Environ. 616-617 (2018) 1242–1260, https://doi.org/10.1016/j.scitotenv.2017.10.193.

[25] Y. Yao, B. Gao, M. Inyang, A.R. Zimmerman, X. Cao, P. Pullammanappallil, et al., Biochar derived from anaerobically digested sugar beet tailings: characterization and phosphate removal potential, Bioresour. Technol. 102 (2011) 6273–6278, https://doi.org/10.1016/j.biortech.2011.03.006.

[26] Y. Yao, B. Gao, J. Chen, L. Yang, Engineered biochar reclaiming phosphate from aqueous solutions: mechanisms and potential application as a slow-release fertilizer, Environ. Sci. Technol. 47 (2013) 8700–8708, https://doi.org/10.1021/es4012977.

[27] Y. Yao, B. Gao, M. Inyang, A.R. Zimmerman, X. Cao, P. Pullammanappallil, et al., Removal of phosphate from aqueous solution by biochar derived from anaerobically digested sugar beet tailings, J. Hazard. Mater. 190 (2011) 501–507, https://doi.org/10.1016/j.jhazmat.2011.03.083.

[28] H. Liu, J. Shan, Z. Chen, E. Lichtfouse, Efficient recovery of phosphate from simulated urine by Mg/Fe bimetallic oxide modified biochar as a potential resource, Sci. Total Environ. 784 (2021) 147546, https://doi.org/10.1016/j.scitotenv.2021.147546.

[29] H. Shin, D. Tiwari, D.-J. Kim, Phosphate adsorption/desorption kinetics and P bioavailability of Mg-biochar from ground coffee waste, J. Water Process Eng. 37 (2020), https://doi.org/10.1016/j.jwpe.2020.101484.

[30] H. Samaraweera, A. Sharp, J. Edwards, C.U. Pittman, X. Zhang, E.B. Hassan, et al., Lignite, thermally-modified and Ca/Mg-modified lignite for phosphate remediation, Sci. Total Environ. 773 (2021) 145631, https://doi.org/10.1016/j.scitotenv.2021.145631.

[31] R. Li, J.J. Wang, B. Zhou, Z. Zhang, S. Liu, S. Lei, et al., Simultaneous capture removal of phosphate, ammonium and organic substances by MgO impregnated biochar and its potential use in swine wastewater treatment, J. Clean. Prod. 147 (2017) 96–107, https://doi.org/10.1016/j.jclepro.2017.01.069.

[32] D. Jiang, B. Chu, Y. Amano, M. Machida, Removal and recovery of phosphate from water by Mg-laden biochar: batch and column studies, Colloids Surf. A Physicochem. Eng. Asp. 558 (2018) 429–437, https://doi.org/10.1016/j.colsurfa.2018.09.016.

[33] S.Y. Lee, J.-W. Choi, K.G. Song, K. Choi, Y.J. Lee, K.-W. Jung, Adsorption and mechanistic study for phosphate removal by rice husk-derived biochar functionalized with Mg/Al-calcined layered double hydroxides via co-pyrolysis, Compos. Part B Eng. 176 (2019), https://doi.org/10.1016/j.compositesb.2019.107209.

[34] D. Zhu, H. Yang, X. Chen, W. Chen, N. Cai, Y. Chen, et al., Temperature-dependent magnesium citrate modified formation of MgO nanoparticles biochar composites with efficient phosphate removal, Chemosphere 274 (2021), https://doi.org/10.1016/j.chemosphere.2021.129904.

[35] R. Li, Q. Zhu, S. Lu, Adsorption of phosphate in water by defective UiO-66/Ce2 $(CO_3)3$ composite: adsorption characteristics and mechanisms, Appl. Surf. Sci. 640 (2023), https://doi.org/10.1016/j.apsusc.2023.158459.

[36] W.-X. Liang, Y. Wei, M. Qiao, J.-W. Fu, J.-X. Wang, High-gravity-assisted controlled synthesis of lanthanum carbonate for highly-efficient adsorption of phosphate, Sep. Purif. Technol. 307 (2023), https://doi.org/10.1016/j.seppur.2022.122696.

[37] H. Li, Y. Wang, Y. Zhao, L. Wang, J. Feng, F. Sun, Efficient simultaneous phosphate and ammonia adsorption using magnesium-modified biochar beads and their recovery performance, J. Environ. Chem. Eng. 11 (2023), https://doi.org/10.1016/j.jece.2023.110875.

[38] B. Wang, W. Zhang, L. Li, W. Guo, J. Xing, H. Wang, et al., Novel talc encapsulated lanthanum alginate hydrogel for efficient phosphate adsorption and fixation, Chemosphere 256 (2020) 127124, https://doi.org/10.1016/j.chemosphere.2020.127124.

[39] C. Feng, L. Zhang, X. Zhang, J. Li, Y. Li, Y. Peng, et al., Bio-assembled MgO-coated tea waste biochar efficiently decontaminates phosphate from water and kitchen waste fermentation liquid, Biochar 5 (2023), https://doi.org/10.1007/s42773-023-00214-0.

[40] L. Kong, Y. Tian, Z. Pang, X. Huang, M. Li, N. Li, et al., Needle-like Mg-La bimetal oxide nanocomposites derived from periclase and lanthanum for cost-effective phosphate and fluoride removal: characterization, performance and mechanism, Chem. Eng. J. 382 (2020) 122963, https://doi.org/10.1016/j.cej.2019.122963.

[41] M. Mallet, K. Barthélémy, C. Ruby, A. Renard, S. Naille, Investigation of phosphate adsorption onto ferrihydrite by X-ray photoelectron spectroscopy, J. Colloid Interface Sci. 407 (2013) 95–101, https://doi.org/10.1016/j.jcis.2013.06.049.

[42] C. Fang, T. Zhang, P. Li, R.-f Jiang, Y.-c Wang, Application of magnesium modified corn biochar for phosphorus removal and recovery from swine wastewater, Int. J. Environ. Res. Public Health 11 (2014) 9217–9237, https://doi.org/10.3390/ijerph110909217.

[43] K. Xu, C. Zhang, X. Dou, W. Ma, C. Wang, Optimizing the modification of wood waste biochar via metal oxides to remove and recover phosphate from human urine, Environ. Geochem. Health 41 (2019) 1767–1776, https://doi.org/10.1007/s10653-017-9986-6.

[44] B. Pan, J. Wu, B. Pan, L. Lv, W. Zhang, L. Xiao, et al., Development of polymer-based nanosized hydrated ferric oxides (HFOs) for enhanced phosphate removal from waste effluents, Water Res. 43 (2009) 4421–4429, https://doi.org/10.1016/j.watres.2009.06.055.

[45] X. Liu, F. Shen, X. Qi, Adsorption recovery of phosphate from aqueous solution by CaO-biochar composites prepared from eggshell and rice straw, Sci. Total Environ. 666 (2019) 694–702, https://doi.org/10.1016/j.scitotenv.2019.02.227.

[46] A. Beatrice, J.J. Varco, A. Dygert, F.S. Atsar, S. Solomon, R. Thirumalai, et al., Lead immobilization in simulated polluted soil by Douglas fir biochar-supported phosphate, Chemosphere 292 (2022) 133355, https://doi.org/10.1016/j.chemosphere.2021.133355.

[47] H. Wang, W. Zhao, Y. Chen, Y. Li, Nickel aluminum layered double oxides modified magnetic biochar from waste corncob for efficient removal of acridine orange, Bioresour. Technol. 315 (2020) 123834, https://doi.org/10.1016/j.biortech.2020.123834.

[48] K. Xu, F. Lin, X. Dou, M. Zheng, W. Tan, C. Wang, Recovery of ammonium and phosphate from urine as value-added fertilizer using wood waste biochar loaded with magnesium oxides, J. Clean. Prod. 187 (2018) 205–214, https://doi.org/10.1016/j.jclepro.2018.03.206.

[49] X. Tao, T. Huang, B. Lv, Synthesis of Fe/Mg-biochar nanocomposites for phosphate removal, Materials 13 (2020), https://doi.org/10.3390/ma13040816.

[50] M. Ghaedi, A. Hassanzadeh, S.N. Kokhdan, Multiwalled carbon nanotubes as adsorbents for the kinetic and equilibrium study of the removal of Alizarin Red S and Morin, J. Chem. Eng. Data 56 (2011) 2511–2520, https://doi.org/10.1021/je2000414.

[51] M. Zhang, B. Gao, Y. Yao, Y. Xue, M. Inyang, Synthesis of porous MgO-biochar nanocomposites for removal of phosphate and nitrate from aqueous solutions, Chem. Eng. J. 210 (2012) 26–32, https://doi.org/10.1016/j.cej.2012.08.052.

[52] W. Deng, D. Zhang, X. Zheng, X. Ye, X. Niu, Z. Lin, et al., Adsorption recovery of phosphate from waste streams by Ca/Mg-biochar synthesis from marble waste, calcium-rich sepiolite and bagasse, J. Clean. Prod. 288 (2021), https://doi.org/10.1016/j.jclepro.2020.125638.

[53] A. Manyatshe, Z.E.D. Cele, M.O. Balogun, T.T.I. Nkambule, T.A.M. Msagati, Chitosan modified sugarcane bagasse biochar for the adsorption of inorganic phosphate ions from aqueous solution, J. Environ. Chem. Eng. 10 (2022), https://doi.org/10.1016/j.jece.2022.108243.

[54] C. Gerente, V. Lee, P. Le Cloirec, G. McKay, Application of chitosan for the removal of metals from wastewaters by adsorption - mechanisms and models review, Crit. Rev. Environ. Sci. Technol. Vol.37 (2007) 41–127, https://doi.org/10.1080/10643380600729089.

[55] J. Li, B. Li, H. Huang, X. Lv, N. Zhao, G. Guo, et al., Removal of phosphate from aqueous solution by dolomite-modified biochar derived from urban dewatered sewage sludge, Sci. Total Environ. 687 (2019) 460–469, https://doi.org/10.1016/j.scitotenv.2019.05.400.

[56] M. Zhang, G. Song, D.L. Gelardi, L. Huang, E. Khan, O. Mašek, et al., Evaluating biochar and its modifications for the removal of ammonium, nitrate, and phosphate in water, Water Res. 186 (2020) 116303, https://doi.org/10.1016/j.watres.2020.116303.

[57] H.N. Tran, E.C. Lima, R. Juang, J.C. Bollinger, H. Chao, Thermodynamic parameters of liquid–phase adsorption process calculated from different equilibrium constants related to adsorption isotherms: a comparison study, J. Environ. Chem. Eng. Vol.9 (2021) 106674, https://doi.org/10.1016/j.jece.2021.106674.

[58] H. Li, S. Mahyoub, W. Liao, S. Xia, H. Zhao, M. Guo, et al., Effect of pyrolysis temperature on characteristics and aromatic contaminants adsorption behavior of magnetic biochar derived from pyrolysis oil distillation residue, Bioresour. Technol. Vol.223 (2017) 20–26, https://doi.org/10.1016/j.biortech.2016.10.033.

[59] J. Liu, M. Zheng, C. Wang, C. Liang, Z. Shen, K. Xu, A green method for the simultaneous recovery of phosphate and potassium from hydrolyzed urine as value-added fertilizer using wood waste, Resour. Conserv. Recycl. 157 (2020), https://doi.org/10.1016/j.resconrec.2020.104793.

[60] Z. Xu, C. Zhang, C. Zhang, Z. Chen, Quantitative evaluation on phosphate adsorption by modified biochar: a meta-analysis, Process Saf. Environ. Prot. 177 (2023) 42–51, https://doi.org/10.1016/j.psep.2023.06.063.

[61] H. Liang, W. Wang, H. Liu, X. Deng, D. Zhang, Y. Zou, et al., Porous MgO-modified biochar adsorbents fabricated by the activation of Mg(NO3)2 for phosphate removal: synergistic enhancement of porosity and active sites, Chemosphere 324 (2023), https://doi.org/10.1016/j.chemosphere.2023.138320.

[62] W. Huang, Y. Zhang, D. Li, Adsorptive removal of phosphate from water using mesoporous materials: a review, J. Environ. Manag. 193 (2017) 470–482, https://doi.org/10.1016/j.jenvman.2017.02.030.

[63] Z. Hu, R. Wu, X. Pang, C. Yu, X. Jian, Adsorption of phosphorus in water by metal-modified large-size biochar: Realizing the recovery and recycling of phosphorus, Sustain. Chem. Pharm. 36 (2023), https://doi.org/10.1016/j.scp.2023.101279.

[64] H. Luo, Y. Wan, Y. Cai, Z. Dang, H. Yin, Enhanced phosphate adsorption by Mg-stirred leaf biochar in a complex water matrix via active MgO facet exposure, ACS EST Eng. Vol.2 (2022) 2254–2265, https://doi.org/10.1021/acsestengg.2c00212.

[65] Y. Yao, B. Gao, J. Chen, M. Zhang, M. Inyang, Y. Li, et al., Engineered carbon (biochar) prepared by direct pyrolysis of Mg-accumulated tomato tissues: characterization and phosphate removal potential, Bioresour. Technol. Vol.138 (2013) 8–13, https://doi.org/10.1016/j.biortech.2013.03.057.

[66] J. Jena, T. Das, U.C. Sarkar, Explicating proficiency of waste biomass-derived biochar for reclaiming phosphate from source-separated urine and its application as a phosphate biofertilizer(Article), J. Environ. Chem. Eng. Vol.9 (2021) 104648, https://doi.org/10.1016/j.jece.2020.104648.

[67] J. Yang, J. Shi, L. Jiang, S. Zhang, F. Wei, Z. Guo, et al., Co-occurrence network in core microorganisms driving the transformation of phosphorous fractionations during phosphorus recovery product used as soil fertilizer, Sci. Total Environ. 871 (2023), https://doi.org/10.1016/j.scitotenv.2023.162081.

[68] T. Zhang, X. He, Y. Deng, D.C.W. Tsang, R. Jiang, G.C. Becker, et al., Phosphorus recovered from digestate by hydrothermal processes with struvite crystallization and its potential as a fertilizer, Sci. Total Environ. 698 (2020), https://doi.org/10.1016/j.scitotenv.2019.134240.

[69] H. Wei, X. Li, W. He, Y. Kuang, Z. Wang, W. Hu, et al., Arbuscular mycorrhizal symbiosis enhances perennial ryegrass growth during temperature stress through the modulation of antioxidant defense and hormone levels, Ind. Crops Prod. 195 (2023), https://doi.org/10.1016/j.indcrop.2023.116412.

[70] Q. Shi, Z. Liu, W. Gao, J. Yan, S. Yuan, H. Liang, et al., Identification of heat tolerance and screening of heat tolerance indexes in different Chinese cabbage seedlings, Sci. Hortic. 322 (2023), https://doi.org/10.1016/j.scienta.2023.112381.

[71] P. Sale, E. Tavakkoli, R. Armstrong, N. Wilhelm, C. Tang, J. Desbiolles, et al., Chapter six: ameliorating dense clay subsoils to increase the yield of rain-fed crops, Adv. Agron. Vol.165 (2021) 249–300, https://doi.org/10.1016/bs.agron.2020.08.003.

[72] S. Maisyarah, J.-Y. Chen, Z.-Y. Hseu, S.-H. Jien, Retention and loss pathways of soluble nutrients in biochar-treated slope land soil based on a rainfall simulator, Soil Environ. Health 1 (2023), https://doi.org/10.1016/j.seh.2023.100021.

[73] B. Wang, Y. Ma, X. Lee, P. Wu, F. Liu, X. Zhang, et al., Environmental-friendly coal gangue-biochar composites reclaiming phosphate from water as a slow-release fertilizer, Sci. Total Environ. 758 (2021), https://doi.org/10.1016/j.scitotenv.2020.143664.

[74] P. Photiou, I. Vyrides, Recovery of phosphate from dewatered anaerobic sludge and wastewater by thermally treated P.oceanica residues and its potential application as a fertilizer, J. Environ. Manag. 298 (2021), https://doi.org/10.1016/j.jenvman.2021.113441.

[75] J.-T. Lee, J.-Y. Son, Y.-S. Cho, The adverse effects of fine particle air pollution on respiratory function in the elderly, Sci. Total Environ. Vol.385 (2007) 28–36, https://doi.org/10.1016/j.scitotenv.2007.07.005.

[76] N. S, S. V, K. N, C. D, A. A, C. S, et al., Sustainable biochar: a facile strategy for soil and environmental restoration, energy generation, mitigation of global climate change and circular bioeconomy, Chemosphere Vol.293 (2022) 133474, https://doi.org/10.1016/j.chemosphere.2021.133474.

[77] M.A. Carneiro, Current trends of arsenic adsorption in continuous mode: literature review and future perspectives, Sustainability Vol.13 (2021) 1186, https://doi.org/10.3390/su13031186.

[78] C. Luerssen, O. Gandhi, T. Reindl, C. Sekhar, D. Cheong, Life cycle cost analysis (LCCA) of PV-powered cooling systems with thermal energy and battery storage for off-grid applications, Appl. Energy Vol.273 (2020) 115145, https://doi.org/10.1016/j.apenergy.2020.115145.

[79] B. Dutta, V. Raghavan, A life cycle assessment of environmental and economic balance of biochar systems in Quebec, Int J. Energy Environ. Eng. Vol.5 (2014), https://doi.org/10.1007/s40095-014-0106-4.

[80] R.A. Reza, J.K. Ahmed, A.K. Sil, M. Ahmaruzzaman, A non-conventional adsorbent for the removal of clofibric acid from aqueous phase, Sep. Sci. Technol. Vol.49 (2014) 1592–1603, https://doi.org/10.1080/01496395.2014.894060.

[81] K. PS, K. L, vL. MCM, W. GJ, Adsorption as a technology to achieve ultra-low concentrations of phosphate: research gaps and economic analysis, Water Res. X Vol.4 (2019) 100029, https://doi.org/10.1016/j.wroa.2019.100029.

[82] F.M. Santos, J. Pires, C.M. eacute, Nutrient recovery from wastewaters by microalgae and its potential application as bio-char, Bioresour. Technol. Vol.267 (2018) 725–731, https://doi.org/10.1016/j.biortech.2018.07.119.

[83] L. Corominas, D.M. Byrne, J.S. Guest, A. Hospido, P. Roux, A. Shaw, et al., The application of life cycle assessment (LCA) to wastewater treatment: a best practice guide and critical review, Water Res. Vol.184 (2020) 116058, https://doi.org/10.1016/j.watres.2020.116058.

Supplementary Material

Efficient recovery of phosphate from urine using magnesite modified corn straw biochar and its sustainable application in fertilizer

Yige Zhou[a], Zehui Liu[a], Jinhua Shan[a], Chengyang Wu[a], Eric Lichtfouse[b], Hongbo Liu[*a]

[a] School of Environment and Architecture, University of Shanghai for Science and Technology, 516 Jungong Road, 200093, Shanghai, China

[b] State Key Laboratory of Multiphase Flow in Power Engineering, Xi'an Jiaotong University, Xi'an, Shaanxi,710049 P.R. China. ORCID: 0000-0002-8535-8073

*Corresponding authors: Hongbo Liu. E-mail: Liuhb@usst.edu.cn (H., Liu) Tel: +86(21)55275979; Fax: +86(21)55275979
Corresponding author ADD: 516, Jungong Road, 200093, Shanghai, China

Text S1 Simulated urine

Actual human urine was obtained from the Institute of Environment of Shanghai University of Technology, and the physicochemical properties of the urine were monitored and recorded during storage at room temperature. In view of the unstable nature of the actual urine, simulated urine distribution was used in all subsequent adsorption sequential batch experiments. Based on the monitoring results of the real urine combined with the relevant academic literature on urine resource utilization, the simulated urine water sample configuration method used in this study was determined as shown in Table S1.

Text S2 Measurement of the point of zero charge (pH_{pzc}) of Mg-biochar

Take 25ml of 0.01mol/l $NaNO_3$ solution and add it to a 50ml centrifuge tube. Adjust the pH value of the solution in the test tube to 3–11 using 0.1mol/L NaOH and HNO_3. Take 0.05g Mg-biochar and add it to the pH adjusted solution. Close the lid and place it in a constant temperature shaker (25 ℃, 125 rpm). After shaking for 24 hours, let the solution in each centrifuge tube pass through the membrane and measure the final pH (pH_f) of the filtrate in each tube using a pH Electrode. Plot pH_i and ΔpH (pH_i -pH_f), where ΔpH=0 represents zero charge point (pH_{pzc}) of Mg-biochar.

Text S3 Experimental measurement of Pot experiments

Determination of plant germination and plant height: 20 seeds were counted and the final number of seeds germinated to calculate the germination rate. The height of the plant was measured above the soil. Three parallel groups were averaged.

Determination of phosphorus content in soil: Place 0.2 g of the dried soil sample in a clean 50 mL centrifuge tube, add 20 mL of 1.0 mol/L KCl solution using a pipette, transfer the tube tightly to a constant temperature shaking incubator and shake it at 25 ℃ for 16 h. After shaking, the tube was transferred to a centrifuge for 15 min at 4500 r/min and removed. The supernatant after centrifugation was filtered through a 0.45 μm membrane, and then the ammonia nitrogen concentration was measured by molybdate spectrophotometry.

Determination of ammonia nitrogen in soil: Place 0.2 g of the dried soil sample in a clean 50 mL centrifuge tube, add 20 mL of 1.0 mol/L hydrochloric acid solution using a pipette, transfer the tube tightly to a constant temperature shaking incubator and shake at 25 ℃ for 16 h. After shaking, the tube was transferred to a centrifuge for 15 min at 4500 r/min and removed. The supernatant after centrifugation was filtered through a 0.45 μm filter membrane and the concentration of ammonia nitrogen was measured spectrophotometrically using a nano reagent.

Text S4 Economic feasibility of Mg-biochar

In this study, all values are converted from RMB to USD (1 USD=7.3 RMB) for comparison with other values in the literature. A tube furnace (1.5 kWh) was used to prepare Mg-biochar with a pyrolysis time of 3 hours. The electricity price in Yangpu District, Shanghai, was 0.09 USD/(kWh). No deionized water was consumed throughout the experiment, and the amount of public laboratory N_2 could not be specifically estimated. The unit price of straw powder purchased from the Internet is 0.55 USD/kg, while in reality, due to the large amount of straw waste, its price is almost zero. The industrial price of magnesite is about 5,000–25,000 RMB/t, and at 25,000 RMB/t, the unit price of magnesite is obtained as 3.43 USD/kg. The yield of Mg-biochar in this study is high, with 10g mixed raw material producing about 9g finished product, a yield of about 90%. In summary, it can be calculated that the cost of producing Mg-biochar is about 2.6 USD/kg.

Table S1 Composition of simulated urine

Component	Unit	Content
pH	-	6.53
NH_4Cl	g/L	0.021
KH_2PO_4	g/L	0.187
$Na_2HPO_4·12H_2O$	g/L	1.155
NaCl	g/L	2.500
Na_2SO_4	g/L	0.980
KCl	g/L	1.146
$CaCl_2$	g/L	0.075
$MgCl_2·6H_2O$	g/L	0.050
Microelement	mL/L	1.0

Table S2 Adsorption model and expression

Model	Expression
Pseudo-first-order kinetic	$q_t = q_e(1 - e^{-k_1 t})$
Pseudo-second-order kinetic	$q_t = \frac{k_2 q_e^2 t}{1 + k_2 q_e t}$
Intra-particle diffusion model	$q_t = k_p t^{1/2} + C$
Langmuir	$q_e = \frac{q_m k_L C_e}{1 + k_L C_e}$
Freundlich	$q_e = k_F C_e^{1/n}$
Sips	$q_e = \frac{q_m k_S C_e^{1/n}}{1 + k_S C_e^{1/n}}$
Temkin	$q_e = a \ln(k_T C_e)$

Table S3 Fitting parameters for the Mg-biochar adsorption kinetics and the isotherm model

Model	Parameter 1	Parameter 2	Parameter 3	R^2
		Adsorption kinetics		
The pseudo-first-order dynamics	k_1=0.743	q_m=114.774	-	0.978
The pseudo-secondary dynamics	k_2=0.007	q_m=127.778	-	0.982
	k_{p1}=51.94	b_1= 1.434	-	0.945
The intra-particle diffusion model	k_{p2}=19.47	b_2= 62.883	-	0.955
	k_{p3}=0.733	b_3= 113.997	-	0.999
		Adsorption isotherm		
Langmuir	k_L=0.093	q_m=197.190	-	0.949
Freundlich	k_F=43.830	n=3.146	-	0.817
Sips	k_S=0.040	q_m=176.156	n=0.670	0.966
Temkin	k_T=0.918	A=41.456	-	0.916

Table S4 Fitting parameters for the biochar (control) adsorption kinetics and the isotherm model

Model	Parameter 1	Parameter 2	Parameter 3	R^2
		Adsorption kinetics		
The pseudo-first-order dynamics	k_1=2.02	q_m=1.125	-	0.841
The pseudo-secondary dynamics	k_2=1.814	q_m=1.102	-	0.085
		Adsorption isotherm		
Langmuir	k_L=0.015	q_m=1.335	-	0.71
Freundlich	k_F=0.151	n=2.800	-	0.95
Sips	k_S=0.741	q_m=2	n=-5.443	-0.001
Temkin	k_T=7.380	A=0.126	-	0.687

Table S5 Cost analysis of Mg-biochar preparation in this study

Type	Inventory	Quantity	Unit	Price (USD)
Output	Mg-biochar	1	kg	2.6
Raw materials	Corn straw	555.6	g	0.30
Raw materials	Magnesite	555.6	g	1.91
Energy	Electronic	4.5	kWh	0.39
Energy	Water	0	L	-
Raw materials	N_2	3	h	-
Environmental emission	CO_2	-	kg	-